JACS JOURNAL OF THE AMERICAN CHEMICAL SOCIETY

Article

Cite This: J. Am. Chem. Soc. 2018, 140, 4543−4551

pubs.acs.org/JACS

Atomistic Mechanism of Large-Scale Conformational Transition in a Heterodimeric ABC Exporter

Hendrik Göddeke,[†] M. Hadi Timachi,[‡] Cedric A. J. Hutter,[§] Laura Galazzo,[‡] Markus A. Seeger,[§] Mikko Karttunen,[∥] Enrica Bordignon,[‡] and Lars V. Schäfer*[,†]

[†]Theoretical Chemistry, Faculty of Chemistry and Biochemistry, Ruhr-University Bochum, 44780 Bochum, Germany

[‡]EPR Spectroscopy, Faculty of Chemistry and Biochemistry, Ruhr-University Bochum, 44780 Bochum, Germany

[§]Institute of Medical Microbiology, University of Zürich, 8006 Zürich, Switzerland

[∥]Department of Chemistry and Department of Applied Mathematics, Western University, London, Ontario N6A 3K7, Canada

Supporting Information

ABSTRACT: ATP-binding cassette (ABC) transporters are ATP-driven molecular machines, in which ATP binding and hydrolysis in the nucleotide-binding domains (NBDs) is chemomechanically coupled to large-scale, alternating access conformational changes in the transmembrane domains (TMDs), ultimately leading to the translocation of substrates across biological membranes. The precise nature of the structural dynamics behind the large-scale conformational transition as well as the coupling of NBD and TMD motions is still unresolved. In this work, we combine all-atom molecular dynamics (MD) simulations with electron paramagnetic resonance (EPR) spectroscopy to unravel the atomic-level mechanism of the dynamic conformational transitions underlying the functional working cycle of the heterodimeric ABC exporter TM287/288. Extensive multimicrosecond simulations in an explicit membrane/water environment show how in response to ATP binding, TM287/288 undergoes spontaneous conformational transitions from the inward-facing (IF) state via an occluded (Occ) intermediate to an outward-facing (OF) state. The latter two states have thus far not been characterized at atomic level. ATP-induced tightening of the NBD dimer involves closing and reorientation of the two NBD monomers concomitant with a closure of the intracellular TMD gate, which leads to the occluded state. Subsequently, opening at the extracellular TMD gate yields the OF conformer. The obtained mechanism imposes NBD-TMD coupling via a tight orchestration of conformational transitions, between both the two domains and also within the TMDs, ensuring that the cytoplasmic and periplasmic gate regions are never open simultaneously.

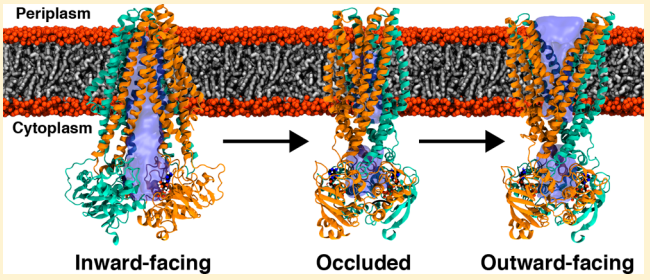

INTRODUCTION

ATP-binding cassette (ABC) transporters are ATP-driven molecular machines that translocate substrates across biological membranes.[1−3] They are found in all kingdoms of life and can be classified into importers and exporters. While ABC importers are unique to bacteria, ABC exporters are found in every organism and transport a wide range of substrates, such as peptides, lipids, or drugs, including chemotherapeutics. Malfunction of ABC exporters is linked to hereditary diseases, such as cystic fibrosis and neonatal diabetes,[4,5] and multidrug resistance of cancer cells and bacteria.[6,7]

At the structural level, all ABC transporters have a core with a common general architecture: a dimer of two nucleotide-binding domains (NBDs) is connected to a dimer of two transmembrane domains (TMDs). The NBDs contain conserved structural motifs that bind and hydrolyze ATP. The free energy gained from ATP binding, hydrolysis, and product dissociation at the NBDs is transmitted to the TMDs, which undergo large-scale alternating access type conformational changes to cycle between an inward-facing (IF) and an outward-facing (OF) state, ultimately leading to substrate translocation.

At a more detailed level, however, different ABC subfamilies can differ substantially, in terms of both structure and mechanism.[8,9] While bacterial ABC exporters are often homodimers, the majority of eukaryotic exporters are heterodimers.[10−12] Many heterodimeric ABC exporters feature one consensus and one degenerate nucleotide binding site. In the degenerate site, the catalytic dyad residues comprising of Walker B glutamate and switch histidine that are essential for ATP hydrolysis,[13,14] as well as residues in the ABC signature motif, deviate from the consensus sequence.

Current molecular understanding of ABC exporters is largely based on X-ray crystal structures, recently reviewed by ter Beek and co-workers,[8] which provide static snapshots of different conformations that could play a role in the functional working cycle. However, the mechanism of ABC transporters is

Received: December 7, 2017
Published: March 16, 2018

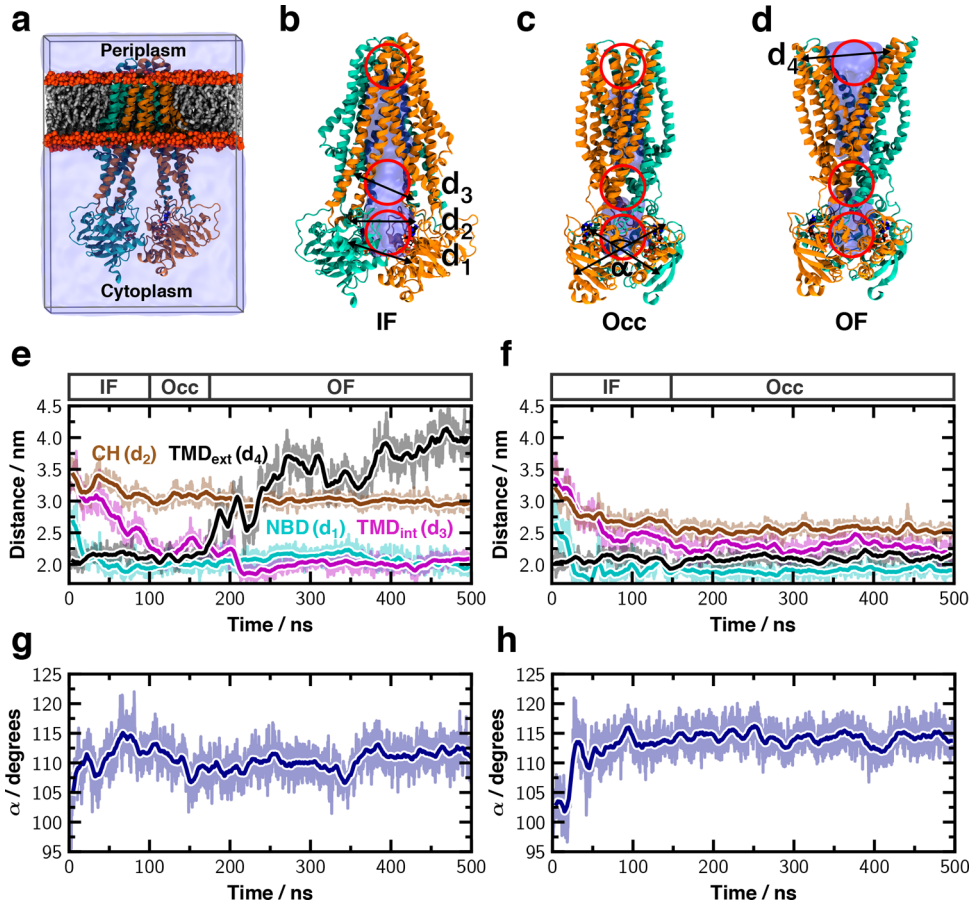

Figure 1. Conformational states of TM287/288 from MD simulations at 375 K. (a) Simulation system with initial inward-facing structure embedded in a solvated lipid bilayer (TM287 orange, TM288 cyan). (b–d) Inward-facing (IF), occluded (Occ), and outward-facing (OF) state. The view in (d) is rotated by 90° along the long axis. The distances d_1, d_2, d_3 and d_4 indicate NBD dimer tightening, movement of the coupling helices (CH), closing of the cytoplasmic TMD gate region (TMD_{int}), and opening of the periplasmic TMD gate (TMD_{ext}), respectively, and were measured between C_α-atoms of residue pairs $D460_{TM287}$–$S363_{TM288}$, $F127_{TM288}$–$T227_{TM288}$, $T131_{TM288}$–$S248_{TM288}$ and $S50_{TM287}$–$S271_{TM287}$, respectively. The blue surfaces visualize the water density inside the TMDs. The red circles indicate the regions used to analyze the changes in hydration of the NBD dimer as well as the cytoplasmic and periplasmic gates upon the conformational transition. (e, f) Time traces of distances d_1 to d_4 during representative IF-to-OF (e) and IF-to-Occ (f) transitions. (g, h) Time traces of NBD twisting angle α during during IF-to-OF (g) and IF-to-Occ (h) transitions; α is the angle between the two vectors connecting the C_α-atoms of residues $L554_{TM287}$–$I452_{TM287}$ and $L576_{TM288}$–$I474_{TM288}$, respectively.

inherently dynamic. In particular, the intricate details of the coupled motions of the NBDs (which dimerize and disengage upon nucleotide binding and unbinding, respectively) and TMDs (which undergo large-scale conformational transitions between the IF and OF states) remain poorly understood at the atomic level.

Molecular dynamics (MD) simulations can provide these missing atomistic insights and hence appear specifically well-suited for studying such membrane protein systems,[15,16] in combination with experimental techniques. However, fully atomistic MD simulations of complete ABC exporters in explicit membrane and water environment are computationally very expensive, and have been carried out only for a few systems, typically covering time scales up to a few hundred nanoseconds.[17−32] Unfortunately, these time scales are usually too short for complete conformational transitions between the IF and OF states to occur spontaneously. This limitation can be addressed by free energy simulations in which transitions are enforced by driving the system along predefined reaction coordinates. Such full-fledged free energy simulations are very demanding, and to our knowledge, a comprehensive free energy profile for an ABC transporter has thus far only been reported in a single study of the homodimeric exporter MsbA.[33] In general, the results of free energy simulations heavily depend on the proper choice of reaction coordinates, which is a highly nontrivial task for systems and conformational transitions as large and complex as ABC transporters. In addition, the artificial biasing forces employed to induce structural transitions in such simulations might have undesired effects on the adopted transition pathways, which could complicate mechanistic interpretations.[34]

The aim of this work is to characterize at the atomic level the full dynamic pathways of the large-scale conformational transitions in an ABC exporter. To that end, instead of using bias potentials to drive the system along preassumed reaction coordinates, we use extensive all-atom MD simulations, totaling more than 50 μs of simulation time, to study the heterodimeric ABC exporter TM287/288 from the thermophilic bacterium *Thermotoga maritima*. TM287/288 is a bacterial homologue of the eukaryotic exporters CFTR,[4] which is linked to cystic fibrosis, and TAP1/2,[35] which transports peptides across the endoplasmic reticulum membrane and is a key player in the

DOI: 10.1021/jacs.7b12944
J. Am. Chem. Soc. 2018, 140, 4543−4551

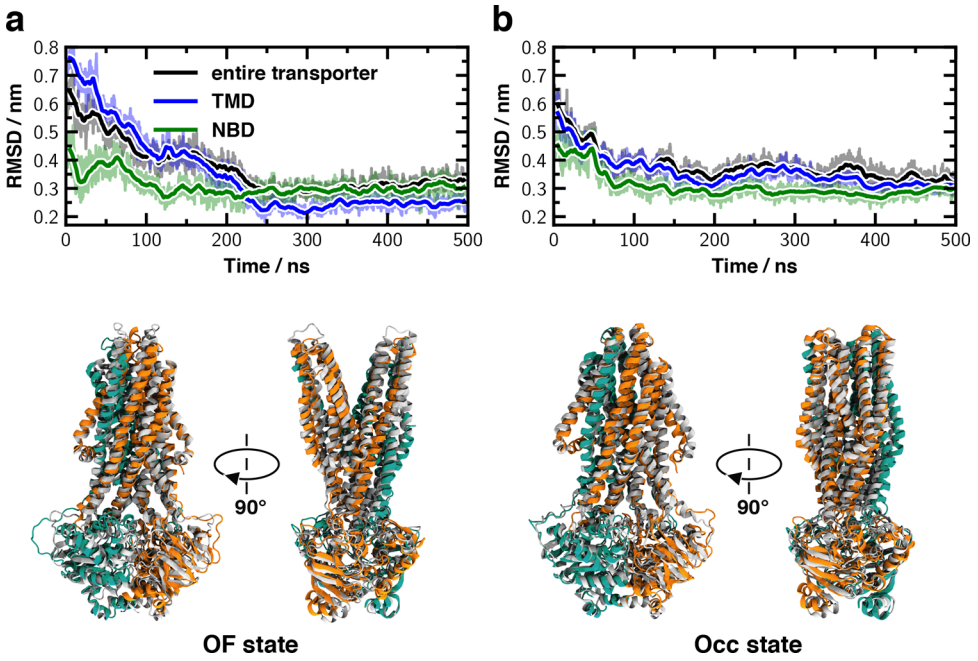

Figure 2. Comparison of the outward-facing and occluded states from the MD simulations to X-ray crystal structures of homologous ABC exporters. (a) Top panel: Root-mean-square deviation (RMSD) of C_α-atoms from the OF crystal structure of Sav1866 (PDB ID code 2HYD) during a representative IF-to-OF simulation. Bottom panel: Structural alignment of the OF state of TM287/288 (snapshot after 500 ns) onto Sav1866 (gray). (b) C_α-RMSD from the PCAT1 crystal structure of the occluded state (PDB ID code 4S0F) during a representative IF-to-Occ simulation. Bottom panel: Structural alignment of the Occ state (snapshot after 500 ns) onto PCAT1 (gray). All structural superposition and RMSD calculations were performed with the *align* function of PyMOL, including a maximum number of 5 outlier rejection cycles. This led to the rejection of up to 10% of the C_α-atoms to mimimize the RMSD.

immune system. Our simulations of TM287/288 are based on the available X-ray crystallography data from Hohl and co-workers[12,36] that show the transporter in an IF state, both for the apo protein and with the nonhydrolyzable ATP analogue adenosine 5′-(*β*,*γ*-imido)triphosphate (AMP-PNP) bound to the degenerate site. As most multidrug efflux proteins, TM287/288 exhibits a basal ATPase activity, i.e., the transporter cycles through its conformational states in a futile manner driven by ATP binding and hydrolysis alone. Substrates such as Hoechst 33342 and daunorubicin increase ATPase activity, but at elevated concentrations they inhibit the process.[12] The IF/OF transition was shown by EPR to be solely triggered by different nucleotides.[37] In this work, we aimed to focus on the protein's conformational transition, therefore we performed the MD simulations in the presence of ATP-Mg but in the absence of substrate. Our MD simulations reveal how TM287/288 loaded with two ATP-Mg molecules, i.e., one ATP-Mg bound to the consensus site in addition to the one bound to the degenerate site, undergoes spontaneous conformational transitions from the known IF state via an occluded intermediate to an OF state; the latter two states had remained elusive so far. Previous EPR studies[37] showed the conformational transition from the IF state to an OF state resembling that of Sav1866 using six spin-labeled pairs in detergent-solubilized transporters. Here we validate the simulated OF structure by EPR using additional spin-labeled pairs in membrane-reconstituted TM287/288. The EPR data corroborates the MD simulations and highlights the role of the membrane bilayer in the stabilization of the extracellular gates. These results allow us to describe the large-scale conformational transition underlying the working cycle of the ABC exporter in atomic detail.

RESULTS AND DISCUSSION

We initiated one hundred 500 ns all-atom MD simulations of TM287/288 from the inward-facing crystal structure with nucleotide bound to the degenerate site.[12,36] In all these simulations, the transporter was inserted into an explicit POPC lipid bilayer and a second ATP-Mg was docked into the consensus site, see Methods. The simulations were carried out at 375 K, because *T. maritima* is extremely thermophilic and grows at temperatures up to 90 °C,[38] hence an increased temperature appears to be a natural choice. In addition, we anticipated that a higher temperature would accelerate structural transitions in our simulations. Control simulations of the apo state and the state in which ATP-Mg is only bound to the degenerate site but not to the consensus site reveal structural stability at 375 K, see Figure S1 in Supporting Information. All results presented are from the simulations at 375 K, unless noted otherwise. Additional control simulations were carried out at 300 K.

In six MD simulations, the transporter transitioned spontaneously from the initial inward-facing (IF) state to an outward-facing (OF) conformation (Figure 1). The observed large-scale conformational transition involves tightening of the NBD dimer and closing of the TMD at the cytoplasmic gate region as well as opening at the periplasmic side. Although the simulations were not guided by any structural information on a target structure, the final OF conformation matches the OF crystal structure of the ABC exporter Sav1866[39] from *S. aureus* (Figure 2). The transition to the OF state proceeded via an occluded (Occ) intermediate state. The latter involves NBD dimer tightening and cytoplasmic TMD closure, but no TMD opening at the periplasmic side (Figure 1). Interestingly, the Occ conformation found in our simulations resembles the

DOI: 10.1021/jacs.7b12944
J. Am. Chem. Soc. 2018, 140, 4543−4551

occluded crystal structures of the ABC exporters PCAT1 from *C. thermocellum*[40] (Figure 2), McjD from *E. coli*,[41] and PglK from *C. jejuni*.[42] In the six simulations in which TM287/288 underwent a complete IF-to-OF transition, the Occ state was visited only transiently along the pathway. However, in 11 other simulations, the transporter transitioned to an Occ state and remained there for the remaining simulation time. In the other 83 simulations, the transporter did not overcome the energy barrier toward Occ during the 500 ns simulation time and remained in the IF state. Furthermore, we initiated 30 additional 500 ns simulations from the OF and Occ state, respectively, after removing ATP-Mg from the two binding sites. However, we did not observe the reverse transitions. One possible explanation for this finding is that the closed NBD dimer, as present in the OF and Occ conformations, is a rather deep free energy minimum and the simulations are thus kinetically trapped on the 500 ns time scale. An alternative explanation could be that ATP hydrolysis, including unbinding of ADP + P_i, is required to drive the reverse transitions. A detailed analysis of these processes would require a quantum mechanical treatment of the chemical reaction steps, which is beyond the scope of this work.

In the following, we describe the structural changes associated with the conformational transitions in more detail; we start with the IF-to-OF transition and then discuss the IF-to-Occ transition. Figure 1a–d show snapshots obtained from our MD simulations at 375 K. Compared to the IF state (Figure 1b), in the OF state the periplasmic and cytoplasmic gates have opened and closed, respectively, and the two NBD monomers have moved toward each other, leading to a tightened NBD dimer (Figure 1d). To analyze this conformational transition in more detail, Figure 1e shows four C_α–C_α distances (d_1 to d_4) between residue pairs during a representative IF-to-OF simulation. The residue pairs for measuring d_1, d_3 and d_4 have been previously shown to be suitable for discriminating between the IF and OF states by EPR;[37] d_2 describes the distance between the coupling helices CH1 and CH2 (i.e., intracellular coupling loops ICL1 and ICL2).

Upon the conformational transition, the NBD dimer tightens as indicated by a change in d_1 by around 0.7 nm (cyan curve). The cytoplasmic (intracellular) region of the TMDs closes by more than 1.5 nm (d_3, magenta curve), whereas the TM helices at the periplasmic (extracellular) TMD gate region open by roughly the same extent (d_4, black curve). The closing motion of the coupling helices (d_2, brown curve) follows that of the cytoplasmic TMD gate region. The conformational transition proceeds in a stepwise fashion; the different milestones along the pathway are indicated by the bars in Figure 1e (top). First, contraction of the NBD dimer (cyan curve) and partial closure of the cytoplasmic TMD gate (magenta curve) occur in a concerted manner. Concomitantly, the two NBD monomers twist with respect to each other; i.e., they change their relative orientation (Figure 1g). These observations underline the collective nature of the coupled conformational motions in the NBDs and TMDs. Furthermore, they are in line with the "doorknob" mechanism,[33] according to which the NBD twist is a prerequisite for subsequent opening/closing TMD motions. Finally, the above initial steps are followed by full closure of the cytoplasmic gate and complete opening of the periplasmic TMD gate (black curve). The other IF-to-OF transitions show a qualitatively similar behavior, see Supporting Information Figure S2. Snapshots of the OF and Occ conformations obtained from the MD simulations are provided as Supporting Information as PDB files.

All transitions to the OF state proceeded via an occluded (Occ) state (Figure 1c and Supporting Information Figures S3, S4). Compared to the complete IF-to-OF transition, transitions from the IF to the Occ state were observed more frequently (in 11 simulations). In those simulations, the structure remained in an Occ conformation, which differs from the OF structure mainly in that the periplasmic gate stays closed (d_4, black curve in Figure 1f). The other distances (d_1 to d_3) as well as the NBD–NBD twisting angle (Figure 1h) change in a qualitatively similar manner as in the IF-to-OF transition.

Currently, there is no published X-ray crystal structure of TM287/288 in an OF state. Thus, to check and validate the OF state found in our simulations, Figure 2a shows a structural alignment to the OF X-ray crystal structure of the homologous ABC exporter Sav1866. The C_α-RMSD to Sav1866 decreases from 0.7 nm to below 0.4 nm in the course of the simulation. The RMSD of the TMDs is on average 0.3 nm, and the RMSD of the NBDs fluctuates to even below 0.2 nm. We assign these low RMSDs to mere thermal fluctuations around a stable OF structure that, at the backbone level, is highly similar to Sav1866, including the complete opening at the periplasmic side. Furthermore, our MD simulations are supported by the agreement of the Occ state obtained from our simulations to the available Occ state X-ray crystal structures of homologous ABC exporters. Figure 2b shows the RMSD and structural alignment to PCAT1[40] as a representative Occ conformation. As discussed above for the similarity of our TM287/288 OF state to the Sav1866 OF X-ray structure, also the Occ conformation identified from the simulations closely matches the available homologous X-ray crystal structure.

Next, to more closely analyze the large-scale conformational transitions, we counted the number of water molecules inside spheres of 1.0 nm radius centered at the cytoplasmic gate, periplasmic gate, and NBD regions (red circles in Figure 1b–d). The results shown in Figure 3 corroborate the concerted conformational transitions described above. The changes in water accessibility of the key structural regions are very pronounced, and hydration hence provides not only a complementary, but maybe an even clearer picture of the conformational transition than the one obtained from analyzing the protein structure alone. Whereas the water count at the cytoplasmic gate region decreases from around 100 to 30 water molecules (Figure 3a, magenta curve), the water count at the periplasmic gate region increases from less than 20 (i.e., almost dry) to about 100 (brown curve). At the same time, the hydration of the NBDs is reduced from 110 to around 80 water molecules. In contrast to the water influx at the periplasmic gate region observed for the OF state, the periplasmic gate in the Occ conformer remains inaccessible to water (Figure 3b, brown curve). Interestingly, the size of the cavity observed in the Occ conformation suffices to harbor one daunorubicin molecule (data not shown). Importantly, the presence of an Occ state ensures that the putative substrate translocation pathway is not simultaneously open to both sides of the membrane. However, the mechanistic implications of rearranging cavity water molecules during substrate translocation remain to be elucidated in more detail.

Finally, we validated the IF to OF transition observed in the MD simulations using distances between spin-labeled pairs in the NBD and TMD regions of the transporter measured by EPR (Figure 4). The IF state was measured in the absence of

DOI: 10.1021/jacs.7b12944
J. Am. Chem. Soc. 2018, 140, 4543–4551

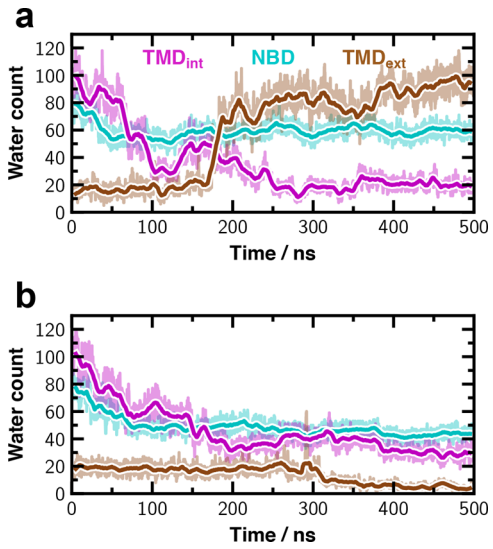

Figure 3. Hydration of the NBDs and the cytoplasmic and periplasmic gate regions during (a) IF-to-OF transition, and (b) IF-to-Occ transition. The number of water molecules inside spheres of radius 1 nm (Figure 2b–d) were counted. For the TMD regions, the sphere centers are defined by the center of mass of the C_α-atoms of 14 residues of each of the four inner TM helices. For the cytoplasmic and periplasmic water analysis, these residues are at the "lower" end of TM helices 3, 4, 9, 10 and "upper" end of TM helices 1, 6, 7, and 12, respectively. For the NBD, the sphere is centered around the lower part of the NBDs and the coupling helices.

nucleotides; the OF-state was induced by trapping of the posthydrolytic intermediate with vanadate and ATP-Mg or binding of ATP-Mg (in case of E517Q mutations), which leads to a predominant population of OF state in detergent-solubilized transporters.[37] Notably, the occluded state could not be experimentally trapped under the investigated conditions.

Figure 4 compares the interspin distances predicted by MMM2015[43] of the apo X-ray structure of TM287/288 (shaded gray histograms) and of the OF state obtained from our MD simulations (average over 20 snapshots, red shaded histograms) with experimental DEER data determined with the transporters in detergent (gray and red solid lines, respectively). Considering the 0.3–0.4 nm intrinsic uncertainty in the modeling of the mean interspin distances,[44] the agreement between simulated and experimental mean distances is good for both NBDs and TMDs (Figure 4c,d and Supporting Information Figure S5). Interestingly, for all three periplasmic TMD pairs, the OF state systematically predicts mean interspin distances about 1 nm longer than those experimentally obtained in detergent (Figure 4a,b and Figure S5). To assess whether the membrane environment, as present in the MD simulations, can affect the opening of the extracellular TMD wings, we reconstituted four spin-labeled pairs of TM287/288 in liposomes and remeasured the distance constraints. In this analysis, the IF distances were found to be invariant in detergent and liposomes (solid and dashed gray lines in Figure 4). Reproducible OF distances were also obtained in the two environments for the NBD and TMD pairs, although their fraction in the overall distribution was decreased due to nonunidirectional insertion of the transporters into liposomes (solid and dashed red lines in Figure 4). Interestingly, in proteoliposomes, a shift toward longer distances was detected at the extracellular region of the transporter, which is in line with the MD simulations. This is reminiscent of what was described for an analogous extracellular spin label pair introduced into the heterodimeric ABC exporter TmrAB.[29]

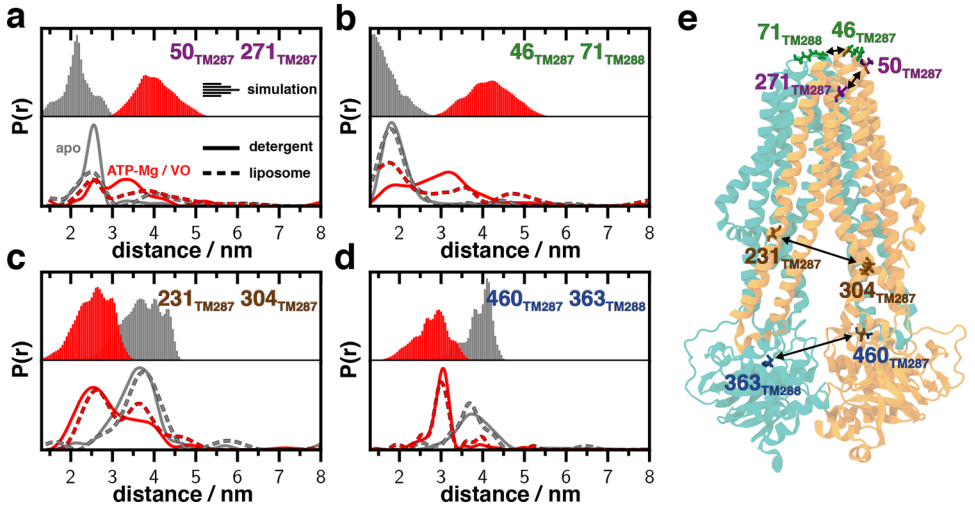

Figure 4. Comparison between simulated OF structure and experimental DEER distance distributions of spin-labeled TM287/288 in detergent and liposomes. (a–d) In the top panels, the gray-shaded histograms show interspin distances simulated using MMM2015 with the room temperature MTSL rotamer library[43] on the apo crystal structure (PDB ID code 4Q4H); the red-shaded histograms result from 20 OF structures obtained from five 500 ns MD simulations at 300 K initiated from the final OF state obtained at 375 K. The distance distributions directly obtained from the 375 K simulations are highly similar (not shown). The bottom panels show experimental distance distributions extracted from high power Q-band DEER traces with DeerAnalysis2015 and normalized by area (1.5–8.0 nm range). (b, c) Spin-labeled pairs in the periplasmic TMDs (46_{TM287}–71_{TM288} and 50_{TM287}–271_{TM287} E517Q). (d, e) Spin-labeled pairs in the NBDs (460_{TM287}–363_{TM288} E517Q) and in the cytoplasmic (TMDs 231_{TM287}–304_{TM287}), respectively. Transporters were solubilized in detergent (solid lines) or reconstituted in liposomes (dashed lines). Gray lines represent apo states and red lines ATP-Mg (E517Q mutant) or ADP-vanadate (VO) states. Detergent data for pairs 460_{TM287}–363_{TM288}, 231_{TM287}–304_{TM287} and 50_{TM287}–271_{TM287}, are shown for comparison only, and were published previously.[37] Primary data and validation of distances are found in Figure S5. (e) Spin-labeled positions in TM287/288.

DOI: 10.1021/jacs.7b12944
J. Am. Chem. Soc. 2018, 140, 4543–4551

Hence, our DEER measurements suggest a more pronounced opening of the extracellular gate in the context of the lipid bilayer, thereby validating the OF state observed in the MD simulations.

The complete transition from the IF to the OF state, in which the TMDs are fully open at the periplasmic side, was observed in only 6 out of 100 conducted MD simulations, whereas the transition from the IF state to the Occ state occurred more frequently (11 times). This difference can have (at least) two possible explanations. First, the simulation time might not suffice to overcome the energy barrier associated with the Occ-to-OF transition in all individual simulations, and hence some simulations are kinetically trapped in the Occ state. A second possible explanation is that the Occ state, and not the OF state, is actually lower in free energy and hence the major populated state when two nucleotides are bound. This alternative is considered unlikely, because it contradicts data on P-gp[28] as well as the available EPR data on TM287/288,[37] which showed that there is a coherent response of the NBDs and TMDs toward an OF state in the presence of different nucleotides and nucleotide analogues in the absence of substrates. However, the conformational equilibria present in TM287/288 (i.e., both IF and OF distances are detected in the presence of nucleotides) may very well include small fractions of occluded conformers in the ensemble. Similar equilibria have been reported for another ABC exporter, TmrAB.[45] Interestingly, recent work on the antibacterial peptide exporter McjD[32] showed that McjD does not adopt a stable open cavity conformation in the presence of ATP and the transported peptide MccJ25, but an outward-occluded structure instead. The bound MccJ25 peptide is released by transient opening of the cavity without large-amplitude motions of the periplasmic TMD gate, hence preventing the influx of the exported toxic peptide.[32] It is well-conceivable that homodimeric McjD and heterodimeric TM287/288 differ in terms of their periplasmic gate motions, however. Although our simulations and EPR data of membrane-reconstituted transporters show that the open OF conformation is possible for TM287/288, further work is needed to unveil the combined conformational motions of substrate and TMDs required for translocation. This formidable endeavor would greatly benefit from computing free energy profiles in the presence of substrate, as discussed below.

The mechanism described in this work agrees with, and to some extent it explains, the ATP switch model[46] in the sense that ATP binding, and not hydrolysis, can suffice to overcome the energy barrier and reach the OF state. In fact, in our MD simulations, introducing a second ATP molecule at the consensus site in addition to the one present in the degenerate site, suffices to trigger the IF-to-OF and IF-to-Occ transitions. ATP hydrolysis and subsequent unbinding of P_i and ADP would thus be required to reset the cycle, allowing the next substrate molecule to be loaded. In a heterodimer, such as TM287/288, this hydrolysis reaction occurs predominantly, if not exclusively, in the consensus site. Therefore, one ATP molecule would (almost) always remain bound to the degenerate site and mediate interactions between the two NBD monomers, which only partially disengage during the working cycle.[36]

CONCLUSIONS

We investigated the large-scale conformational transition between IF and OF states of the heterodimeric ABC exporter TM287/288 using extensive MD simulations in explicit membrane and water environment. The complete, spontaneous transition to the OF state observed in our MD simulations was validated by experimental distances between spin-labeled pairs engineered in membrane-reconstituted transporters. The simulations provide atomic-level insight into the structural dynamics underlying an intricate multistep mechanism, which involves coupled cooperative motions of NBDs and TMDs. First, in the presence of ATP in the nucleotide binding sites, the NBD dimer tightens by a simultaneous closing and twisting motion, i.e., upon approaching each other the two NBD monomers reorient to enable the formation of a fully closed dimer. Concomitantly, the cytoplasmic gate region of the TMDs closes, thereby forming an occluded (Occ) intermediate state. Finally, the periplasmic TMD gate opens, yielding the OF state that is accessible to the other side of the membrane. Our MD results are strongly supported by the similarity of the identified Occ and OF conformations to known X-ray crystal structures of homologous ABC transporters. However, although the agreement to these X-ray structures is apparently very good at the backbone level, full structural relaxation of the formed NBD and TMD interfaces, including the precise arrangement of side-chains, might occur on much longer time scales and thus require even longer simulations.

Full characterization of the complete functional working cycle of an ABC transporter would require sampling the structural dynamics of the IF/OF conformational transition in a reversible manner at equilibrium and, ultimately, to explicitly include substrate (allocrite) molecules and study their actual translocation pathways. This has not been achieved at atomic resolution so far, but our results provide a key step in this direction. In particular, the conformational transitions occur spontaneously in our simulations, thus revealing not only the characteristics of the individual steps involved (e.g., collective conformational transitions in NBDs and TMDs), but also the natural sequence of events. This enables one to extract a small but relevant set of suitable reaction coordinates for subsequent free energy simulations of the IF/OF transition in the presence of a translocated substrate.

METHODS

MD Simulations. All MD simulations were carried out with the GROMACS program package, version 5.1.[47] The Amber ff99sb-ILDN force field[48,49] was used for the protein, together with the Berger lipid parameters[50] for POPC, including the dihedral parameters of Bachar and co-workers[51] for the torsion around the bond adjacent to the cis double bond in the unsaturated hydrocarbon tail; the lipid parameters were obtained from Cordomi and co-workers.[52] For ATP, the force field parameters of Meagher and co-workers[53] were used. The starting structure for the simulations was taken from the 2.6 Å resolution crystal structure of TM287/288 in an inward-facing conformation[12,36] with AMP-PNP bound at the degenerate site (PDB ID code 4Q4A). AMP-PNP was converted into ATP and a second ATP molecule was docked into the consensus site in two steps. First, to get an initial estimate of the position of ATP and the Mg^{2+} ion, the consensus site was superimposed onto the degenerate site by least-squares fitting of one NBD onto the other. Second, on the basis of other crystal structures of ABC transporters with bound ATP,[54−56] the ATP position and coordination of Mg^{2+} was further refined. This refinement included (i) stepwise decreasing the distance between the carbonyl oxygen of Q436 and the Mg^{2+} ion to 2.0 Å (in 0.1 Å steps, each involving steepest descent energy minimization), (ii) rotating the side chain dihedral angle of T395 such that the O_γ-atom is in contact with Mg^{2+}, (iii) rotating the terminal dihedral angle of the K394 side chain to establish two hydrogen bonds with the ATP β- and γ-phosphate groups, and (iv) adding the missing two water molecules into the Mg^{2+}

DOI: 10.1021/jacs.7b12944
J. Am. Chem. Soc. 2018, 140, 4543−4551

coordination shell, yielding a hexa-coordinated Mg^{2+}. Although not explicitly enforced upon docking, the A-loop tyrosine (Y364) forms a proper π-stack to the adenosine moiety in our final structure. The obtained doubly ATP-loaded structure was then embedded into a pre-equilibrated POPC lipid bilayer. As in our previous simulations of BtuCD-F,[57] the inflation-insertion-deflation protocol of Kandt and co-workers[58] was used, and the orientation and insertion depth of the protein in the lipid bilayer was determined with the orientations of proteins in membranes (OPM) web server.[59] The system was solvated with water such that no water molecules were introduced in the hydrocarbon region of the bilayer. The periodic simulation box contained 255 POPC lipids (128 lipids in one leaflet, 127 in the other leaflet), 33 370 TIP4P/2005 water molecules,[60] and Cl^- ions to neutralize the simulation box, yielding a total system size of ca. 132 000 atoms. The box dimensions were ca. 10.3 × 9.8 × 14.6 nm. Prior to the simulations, the system was energy minimized (using steepest descent) and equilibrated for 10 ns in the NpT ensemble with harmonic position restraints on all protein heavy atoms (force constants of 1000 kJ mol^{-1} nm^{-2}), allowing for relaxation of the lipid and water molecules around the protein.

In the MD simulations, short-range nonbonded Coulomb and Lennard-Jones 6−12 interactions were treated with a buffered Verlet pair list[61] with potentials smoothly shifted to zero at a 1.0 nm cutoff. Analytical dispersion corrections were applied for energy and pressure to compensate for the truncation of the Lennard-Jones interactions. Long-range electrostatic interactions were treated with the particle mesh Ewald (PME) method[62,63] with a grid spacing of 0.12 nm and cubic spline interpolation. The SETTLE algorithm[64] was used to constrain the internal degrees of freedom of the water molecules, and LINCS[65] was used to constrain all other bond lengths. Virtual interaction sites were used for the hydrogen atoms,[66] allowing to integrate the equations of motion with 4 fs time steps. The simulations were carried out in the NpT ensemble. Temperature was kept constant at the desired value (300 or 375 K) by coupling to a velocity rescaling thermostat[67] with coupling time constant 0.1 ps. For constant pressure, semi-isotropic coupling was applied by separately coupling the lateral (xy) and normal (z) box directions to a pressure bath at 1 bar using a Berendsen barostat[68] with time constant of 2 ps and compressibility 4.5 × 10^{-5} bar^{-1}. The above setup has been shown to be reliable for simulations of membrane proteins.[69] At 375 K, 100 MD simulations of length 500 ns were initiated from different random seeds for the initial Maxwell velocity distribution. Simulations in which a spontaneous conformational transition to an outward-facing state occurred were extended up to 1 μs. One representative trajectory of an inward-facing to occluded state transition was also extended up to 1 μs. In addition, to investigate the structural dynamics of the inward- and outward-facing states at 300 K, five additional 500 ns simulations were carried out for each conformer at the lower temperature used for EPR validation; these simulations were initiated from the configurations obtained after 600, 700, 800, 900, and 1000 ns of the 1 μs MD simulation at 375 K. To study the properties of the bilayer at 300 and 375 K, additional 500 ns simulations of a pure bilayer (i.e., without protein) comprised of 256 POPC lipids, solvated by 14 966 TIP4P/2005 water molecules, were carried out at these two temperatures. At 300 K, the average area per lipid is 0.63 nm^2. The bilayer is also stable under the simulation conditions at 375 K, with an average area per lipid of 0.70 nm^2.

Spin-Labeled Pairs and Interspin Distance Simulations. Five previously described[37] spin-labeled pairs positioned in the NBDs, as well as in the cytoplasmic and periplasmic TMDs were used. Two new pairs (271_{TM287}−290_{TM288} and 46_{TM287}−71_{TM288}) were created in the periplasmic TMDs for further validation of the OF MD structure with following criteria: strategic position in the periplasmic TMD region, high accessibility toward the aqueous environment, high number of populated rotamers and distinct distances in the inward with respect to the outward-facing models. The new periplasmic pairs were found to be active in detergent (activities normalized to the wildtype: 81.5% (SD 5.6%) for 271_{TM287}−290_{TM288} and 56.2% (SD 2.1%) for 46_{TM287}−71_{TM288}) and in proteoliposomes based on ATPase assays (Supporting Information Figure S6). For the prediction of interspin distances, the inward-facing crystal structure of TM287/288 in its apo state (PDB ID code 4Q4H) and 20 models from our MD simulations at 300 K were used as templates. Distances were simulated using the ambient temperature rotamer library approach for side chains labeled with MTSL ([1-oxyl-2,2,5,5-tetramethyl-Δ3-pyrroline-3-methyl] methanethiosulfonate) available in the Matlab package MMM2015.[43]

Protein Preparation and Reconstitution. The expression, purification and labeling protocol was described in a previous study.[37] Four variants of the transporter were reconstituted into lipid membrane vesicles consisting of polar *E. coli* lipids and egg phosphatidylcholine (Avanti Polar Lipids) mixed at a weight ratio of 3:1. The reconstitution protocol via biobeads (Biorad) followed Geertsma and co-workers[70] with minor modifications: the sonication step before flash-freezing and extrusion was omitted; lipid/protein ratio was 50 (w/w) to optimize the EPR signal-to-noise; proteoliposomes were separated from the biobeads using a Pasteur pipet. The sample was spun down at 15 000g for 20 s to eliminate possible protein precipitate; the supernatant was then concentrated by centrifugation at 150 000g for 1 h at 4 °C.

EPR Sample Preparation. The labeling efficiency of the double cysteine mutants of the transporters solubilized in detergent was measured by comparing the second integral of the continuous wave X-band room temperature EPR spectra with a reference sample of TEMPOL of known concentration (http://www.spintoolbox.com). The calculated spin labeling efficiencies of all investigated mutants ranged between 70 and 90%. For DEER measurements, 10% v/v glycerol-d_8 was added prior to snap freezing. 40 μL of sample were loaded in quartz tubes with 3 mm outer diameter. To populate to OF state, transporters solubilized in detergent (or reconstituted in liposomes) were incubated with 5 mM sodium orthovanadate, 2.5 mM ATP and 2.5 mM $MgCl_2$ at 50 °C for 3 min (4 min), incubated at 25 °C for 1−2 min and snap frozen in liquid nitrogen. To populate the OF state in the spin-labeled mutants engineered in TM287/288 carrying the E517Q mutation, samples were directly incubated with 2.5 mM $MgCl_2$ and 2.5 mM ATP at 25 °C for 8 min (10 min) and snap frozen in liquid nitrogen.

DEER Experiments and Analysis. Double electron−electron resonance (DEER) measurements were performed at 50 K on a Bruker ELEXSYS E580Q-AWG pulse Q-band spectrometer equipped with a 150 W TWT amplifier. A 4-pulse DEER sequence with nonselective observer and pump pulses (12−14 ns and 32−34 ns for rectangular and Gaussian pulses, respectively, depending on the available B_1 at the sample) with 90−100 MHz frequency separation was used. The full width at half-maximum of the Gaussian pulses corresponds to 13−14 ns. Phase cycling (0−π) of all observer pulses was coupled to a 4-step phase cycling (0−π/2−π−3π/2) of the pump π-pulse, to remove unwanted effects of running echoes from the DEER trace due to the coherent nature of the AWG generated pulses. The evaluation and validation of the DEER data was performed using DeerAnalysis2015.[71] The background of the primary DEER traces was corrected using stretched exponential functions with homogeneous dimensions of 2 to 3 for different samples. A model-free Tikhonov regularization was used to extract distance distributions from the background corrected form factors. A validation of the Tikhonov regularization has been performed for the four data sets in liposomes using following trials: background starting point from 400 to 1000 ns with 7 steps and background fit dimension from 2 to 3 with 5 steps. The validation was further refined with an L_{prune} of 1.15 which limits the RMSD deviation of the error estimates from the experimental data to that of the best fit by a factor of L_{prune}.

■ ASSOCIATED CONTENT

Supporting Information

The Supporting Information is available free of charge on the ACS Publications website at DOI: 10.1021/jacs.7b12944.

Control simulations of the apo and singly ATP-loaded structures at 375 K; Additional IF-to-OF and IF-to-Occ conformational transitions not shown in Figure 1;

DOI: 10.1021/jacs.7b12944
J. Am. Chem. Soc. 2018, 140, 4543−4551

Occluded structure transiently visited during the IF-to-OF transition shown in Figure 1e; DEER analysis of spin-labeled TM287/288; Stimulation of ATP hydrolysis by Hoechst 3342 (PDF)
Snapshot (PDB) of OF conformation obtained from MD simulations at 375 K (ZIP)
Snapshot (PDB) of Occ conformation obtained from MD simulations at 375 K (ZIP)

AUTHOR INFORMATION

Corresponding Author

*lars.schaefer@ruhr-uni-bochum.de

ORCID

Lars V. Schäfer: 0000-0002-8498-3061

Notes

The authors declare no competing financial interest.

ACKNOWLEDGMENTS

We thank Gunnar Jeschke (ETH Zürich) for providing the Q-band resonator, Tufa E. Assafa for help in size-exclusion chromatography and Lea M. Hürlimann for ATPase activity assays. The Steinbuch Centre for Computing (SCC) Karlsruhe is acknowledged for providing generous computational resources. This work was funded by the Deutsche Forschungsgemeinschaft (DFG) through an Emmy Noether grant to L.V.S. (SCHA 1574/3-1), Cluster of Excellence RESOLV (EXC 1069), and a research grant to E.B. (BO 3000/1-2). M.K. is supported by the Natural Sciences and Engineering Council of Canada (NSERC) and Canada Research Chairs Program.

REFERENCES

(1) Davidson, A. L.; Dassa, E.; Orelle, C.; Chen, J. *Microbiol. Mol. Biol. Rev.* **2008**, *72*, 317−364.
(2) Rees, D. C.; Johnson, E.; Lewinson, O. *Nat. Rev. Mol. Cell Biol.* **2009**, *10*, 218−227.
(3) Jones, P. M.; O'Mara, M. L.; George, A. M. *Trends Biochem. Sci.* **2009**, *34*, 520−531.
(4) Gadsby, D. C.; Vergani, P.; Csanády, L. *Nature* **2006**, *440*, 477−483.
(5) Aittoniemi, J.; Fotinou, C.; Craig, T. J.; de Wet, H.; Proks, P.; Ashcroft, F. M. *Philos. Trans. R. Soc., B* **2009**, *364*, 257−267.
(6) Gottesman, M. M.; Ling, V. *FEBS Lett.* **2006**, *580*, 998−1009.
(7) Higgins, C. F. *Nature* **2007**, *446*, 749−757.
(8) ter Beek, J.; Guskov, A.; Slotboom, D. J. *J. Gen. Physiol.* **2014**, *143*, 419−435.
(9) Locher, K. P. *Nat. Struct. Mol. Biol.* **2016**, *23*, 487−493.
(10) Venter, H.; Shilling, R. A.; Velamakanni, S.; Balakrishnan, L.; Van Veen, H. W. *Nature* **2003**, *426*, 866−870.
(11) Procko, E.; O'Mara, M. L.; Bennett, W. F. D.; Tieleman, D. P.; Gaudet, R. *FASEB J.* **2009**, *23*, 1287−1302.
(12) Hohl, M.; Briand, C.; Grütter, M. G.; Seeger, M. A. *Nat. Struct. Mol. Biol.* **2012**, *19*, 395−402.
(13) Orelle, C.; Dalmas, O.; Gros, P.; Di Pietro, A.; Jault, J. M. *J. Biol. Chem.* **2003**, *278*, 10824−10834.
(14) Oldham, M. L.; Chen, J. *Proc. Natl. Acad. Sci. U. S. A.* **2011**, *108*, 15152−15156.
(15) Lindahl, E.; Sansom, M. S. P. *Curr. Opin. Struct. Biol.* **2008**, *18*, 425−431.
(16) Li, J.; Wen, P.-C.; Moradi, M.; Tajkhorshid, E. *Curr. Opin. Struct. Biol.* **2015**, *31*, 96−105.
(17) Becker, J.-P.; Van Bambeke, F.; Tulkens, P. M.; Prévost, M. *J. Phys. Chem. B* **2010**, *114*, 15948−15957.
(18) Aittoniemi, J.; De Wet, H.; Ashcroft, F. M.; Sansom, M. S. P. *PLoS Comput. Biol.* **2010**, *6*, e1000762.
(19) Weng, J.-W.; Fan, K.-N.; Wang, W.-N. *J. Biol. Chem.* **2010**, *285*, 3053−3063.
(20) Oliveira, A. S.; Baptista, A. M.; Soares, C. M. *Proteins: Struct., Funct., Genet.* **2011**, *79*, 1977−1990.
(21) O'Mara, M. L.; Mark, A. E. *J. Chem. Theory Comput.* **2012**, *8*, 3964−3976.
(22) St-Pierre, J.-F.; Bunker, A.; Róg, T.; Karttunen, M.; Mousseau, N. *J. Phys. Chem. B* **2012**, *116*, 2934−2942.
(23) Wen, P.-C.; Verhalen, B.; Wilkens, S.; Mchaourab, H. S.; Tajkhorshid, E. *J. Biol. Chem.* **2013**, *288*, 19211−19220.
(24) Shintre, C. A.; Pike, A. C. W.; Li, Q.; Kim, J.-I.; Barr, A. J.; Goubin, S.; Shrestha, L.; Yang, J.; Berridge, G.; Ross, J.; Stansfeld, P. J.; Sansom, M. S P.; Edwards, A. M.; Bountra, C.; Marsden, B. D.; von Delft, F.; Bullock, A. N.; Gileadi, O.; Burgess-Brown, N. A.; Carpenter, E. P. *Proc. Natl. Acad. Sci. U. S. A.* **2013**, *110*, 9710−9715.
(25) O'Mara, M. L.; Mark, A. E. *PLoS One* **2014**, *9*, e91916.
(26) Gu, R.-X.; Corradi, V.; Singh, G.; Choudhury, H. G.; Beis, K.; Tieleman, D. P. *Biochemistry* **2015**, *54*, 5989−5998.
(27) Furuta, T.; Sato, Y.; Sakurai, M. *Biochemistry* **2016**, *55*, 6730−6738.
(28) Verhalen, B.; Dastvan, R.; Thangapandian, S.; Peskova, Y.; Koteiche, H. A.; Nakamoto, R. K.; Tajkhorshid, E.; Mchaourab, H. S. *Nature* **2017**, *543*, 738−741.
(29) Nöll, A.; Thomas, C.; Herbring, V.; Zollmann, T.; Barth, K.; Mehdipour, A. R.; Tomasiak, T. M.; Brüchert, S.; Joseph, B.; Abele, R.; Oliéric, V.; Wang, M.; Diederichs, K.; Hummer, G.; Stroud, R. M.; Pos, K. M.; Tampé, R. *Proc. Natl. Acad. Sci. U. S. A.* **2017**, *114*, E438−E447.
(30) Xu, Y.; Seelig, A.; Bernèche, S. *ACS Cent. Sci.* **2017**, *3*, 250−258.
(31) Das, J.; Aleksandrov, A. A.; Cui, L.; He, L.; Riordan, J. R.; Dokholyan, N. V. *PLoS Comput. Biol.* **2017**, *13*, e1005594.
(32) Bountra, K.; Hagelueken, G.; Choudhury, H. G.; Corradi, V.; El Omari, K.; Wagner, A.; Mathavan, I.; Zirah, S.; Wahlgren, W. Y.; Tieleman, D. P.; Schiemann, O.; Rebuffat, S.; Beis, K. *EMBO J.* **2017**, *36*, 3062−3079.
(33) Moradi, M.; Tajkhorshid, E. *Proc. Natl. Acad. Sci. U. S. A.* **2013**, *110*, 18916−18921.
(34) Latorraca, N. R.; Fastman, N. M.; Venkatakrishnan, A.; Frommer, W. B.; Dror, R. O.; Feng, L. *Cell* **2017**, *169*, 96−107.
(35) Parcej, D.; Tampé, R. *Nat. Chem. Biol.* **2010**, *6*, 572−580.
(36) Hohl, M.; Hürlimann, L. M.; Bohm, S.; Schoppe, J.; Grütter, M. G.; Bordignon, E.; Seeger, M. A. *Proc. Natl. Acad. Sci. U. S. A.* **2014**, *111*, 11025−11030.
(37) Timachi, M. H.; Hutter, C. A.; Hohl, M.; Assafa, T.; Böhm, S.; Mittal, A.; Seeger, M. A.; Bordignon, E. *eLife* **2017**, DOI: 10.7554/eLife.20236.
(38) Huber, R.; Langworthy, T. A.; König, H.; Thomm, M.; Woese, C. R.; Sleytr, U. B.; Stetter, K. O. *Arch. Microbiol.* **1986**, *144*, 324−333.
(39) Dawson, R. J.; Locher, K. P. *Nature* **2006**, *443*, 180−185.
(40) Lin, D. Y.; Huang, S.; Chen, J. *Nature* **2015**, *523*, 425−430.
(41) Choudhury, H. G.; Tong, Z.; Mathavan, I.; Li, Y.; Iwata, S.; Zirah, S.; Rebuffat, S.; Van Veen, H. W.; Beis, K. *Proc. Natl. Acad. Sci. U. S. A.* **2014**, *111*, 9145−9150.
(42) Perez, C.; Gerber, S.; Boilevin, J.; Bucher, M.; Darbre, T.; Aebi, M.; Reymond, J.-L.; Locher, K. P. *Nature* **2015**, *524*, 433−438.
(43) Polyhach, Y.; Bordignon, E.; Jeschke, G. *Phys. Chem. Chem. Phys.* **2011**, *13*, 2356−2366.
(44) Jeschke, G. *Prog. Nucl. Magn. Reson. Spectrosc.* **2013**, *72*, 42−60.
(45) Barth, K.; Hank, S.; Spindler, P. E.; Prisner, T. F.; Tampé, R.; Joseph, B. *J. Am. Chem. Soc.* **2018**, DOI: 10.1021/jacs.7b12409.
(46) Higgins, C. F.; Linton, K. J. *Nat. Struct. Mol. Biol.* **2004**, *11*, 918−926.
(47) Abraham, M. J.; Murtola, M.; Schulz, R.; Páll, S.; Smith, J. C.; Hess, B.; Lindahl, E. *SoftwareX* **2015**, *1−2*, 19−25.
(48) Hornak, V.; Abel, R.; Okur, A.; Strockbine, B.; Roitberg, A.; Simmerling, C. *Proteins: Struct., Funct., Genet.* **2006**, *65*, 712−725.
(49) Lindorff-Larsen, K.; Piana, S.; Palmo, K.; Maragakis, P.; Klepeis, J. L.; Dror, R. O. *Proteins: Struct., Funct., Genet.* **2010**, *78*, 2002−2013.

DOI: 10.1021/jacs.7b12944
J. Am. Chem. Soc. 2018, 140, 4543−4551

(50) Berger, O.; Edholm, O.; Jähnig, F. *Biophys. J.* **1997**, *72*, 2002−2013.
(51) Bachar, M.; Brunelle, P.; Tieleman, D. P.; Rauk, A. *J. Phys. Chem. B* **2004**, *108*, 7170−7179.
(52) Cordomi, A.; Caltabiano, G.; Pardo, L. *J. Chem. Theory Comput.* **2012**, *8*, 948−958.
(53) Meagher, K. L.; Redman, L. T.; Carlson, H. A. *J. Comput. Chem.* **2003**, *24*, 1016−1025.
(54) Korkhov, V.; Mireku, S. A.; Locher, K. P. *Nature* **2012**, *490*, 367−372.
(55) Ward, A.; Reyes, C. L.; Yu, J.; Roth, C. B.; Chang, G. *Proc. Natl. Acad. Sci. U. S. A.* **2007**, *104*, 19005−19010.
(56) Dawson, R. J. P.; Locher, K. P. *FEBS Lett.* **2007**, *581*, 935−938.
(57) Prieß, M.; Schäfer, L. V. *Biophys. J.* **2016**, *110*, 2407−2418.
(58) Kandt, C.; Ash, W. L.; Tieleman, D. P. *Methods* **2007**, *41*, 475−488.
(59) Lomize, M. A.; Pogozheva, I. D.; Joo, H.; Mosberg, H. I.; Lomize, A. L. *Nucleic Acids Res.* **2012**, *40*, D370−D376.
(60) Abascal, J. L. F.; Vega, C. *J. Chem. Phys.* **2005**, *123*, 234505.
(61) Páll, S.; Hess, B. *Comput. Phys. Commun.* **2013**, *184*, 2641−2650.
(62) Darden, T.; York, D.; Pedersen, L. *J. Chem. Phys.* **1993**, *98*, 10089.
(63) Essmann, U.; Perera, L.; Berkowitz, M. L.; Darden, T.; Lee, H.; Pedersen, L. G. *J. Chem. Phys.* **1995**, *103*, 8577−8593.
(64) Miyamoto, S.; Kollman, P. A. *J. Comput. Chem.* **1993**, *13*, 952−962.
(65) Hess, B. *J. Chem. Theory Comput.* **2008**, *4*, 116−122.
(66) Feenstra, K. A.; Hess, B.; Berendsen, H. J. C. *J. Comput. Chem.* **1999**, *20*, 786−798.
(67) Bussi, G.; Donadio, D.; Parrinello, M. *J. Chem. Phys.* **2007**, *126*, 014101.
(68) Berendsen, H. J. C.; Postma, J. P. M.; van Gunsteren, W. F.; DiNola, A.; Haak, J. R. *J. Chem. Phys.* **1984**, *81*, 3684−3690.
(69) Wong-ekkabut, J.; Karttunen, M. *J. Chem. Theory Comput.* **2012**, *8*, 2905−2911.
(70) Geertsma, E. R.; Mahmood, N. N.; Schuurman-Wolters, G. K.; Poolman, B. *Nat. Protoc.* **2008**, *3*, 256−266.
(71) Jeschke, G.; Chechik, V.; Ionita, P.; Godt, A.; Zimmermann, H.; Banham, J.; Timmel, C.; Hilger, D.; Jung, H. *Appl. Magn. Reson.* **2006**, *30*, 473−498.

DOI: 10.1021/jacs.7b12944
J. Am. Chem. Soc. 2018, 140, 4543−4551